Ocean Engineering 123 (2016) 440–451

Contents lists available at ScienceDirect

Ocean Engineering

journal homepage: www.elsevier.com/locate/oceaneng

Numerical investigation of the vertical response of a containership in large amplitude waves

Suresh Rajendran, C. Guedes Soares *

Centre for Marine Technology and Ocean Engineering (CENTEC), Instituto Superior Técnico, Universidade de Lisboa, Portugal

ARTICLE INFO

Article history:
Received 2 August 2015
Received in revised form
7 March 2016
Accepted 26 June 2016
Available online 19 July 2016

Keywords:
Hydroelasticity
Body nonlinear time domain method
Strip theory
Containership
Vertical motion and bending moment
Large amplitude waves

ABSTRACT

The symmetric distortions of a containership in large amplitude waves are analyzed by means of numerical methods and are compared with experimental results. The study is part of a ISSC–ITTC benchmark study which was intended to analyze the accuracy of the numerical methods and the uncertainty involved with the predictions of the ship responses. In this paper the numerical calculations are carried out by means of a body nonlinear time domain method. The time domain code is coupled with a finite element model and the ship hull is modeled as a non-uniform Timoshenko beam. The experiments were conducted in a wave tank with an aluminum back bone and the flexible responses of the ship were measured. The ship was tested in regular waves of moderate to large amplitude to analyze the effect of nonlinear springing. Even though a slight discrepancy is found between the numerical and the experimental vertical motions in large amplitude waves, the numerical vertical bending moments are in reasonably good agreement with the experimental results.

1. Introduction

Increase in demand for longer and larger containerships with capacities varying between 8000 and 14000 TEU and length up to 400 m has reemphasized the importance of hydroelasticity in ship design. Due to their open hull structure and long hulls, containerships are highly susceptible to springing and whipping, among which the former leads to fatigue failure, and the latter is important for structural design as it imparts huge impact load on structure and can also be a cause of fatigue failure. Springing is a phenomenon in which wave frequency or its harmonics are able to resonate at the structural natural frequency, and whipping loads results from slamming of ships which cause transient dynamic loading on ships.

Recently, ISSC 2012 (Drummen and Holtmann, 2014) conducted a benchmark study for slamming and whipping, the main objective of which was to estimate the degree of variation in the results between different numerical methods and their agreement with experimental results. The participants were free to use any method suitable for them. Most of the participants used 3D panel methods for calculation of the added mass and lumped it to the structural model, while a participant coupled the structural solver with a Reynolds Averaged Navier Stokes (RANS) solver. A wide range of methods were used for the structural model, which included 2D beam element with links connecting the mass segment, 2D Timoshenko beam and 3D shell elements. It was concluded that the mode shapes and the natural frequency for two, three node vibration of both dry and wet symmetric and antisymmetric distortion were well estimated by most of the participants. However, more complex methods do not necessarily give good results as the more elaborated models included additional uncertainties.

Ramos et al. (2000) experimentally investigated the slam induced responses of a containership to compare the results with a numerical method. The responses included a vibratory component but the model was not constructed in order to keep the scaling for those responses. However later models with a flexible backbone had that possibility and allowed studies of hydroelastic behavior. Zhu et al. (2011) investigated experimentally the hull girder vibration of a flexible backbone model in bending and torsion. The paper listed the number of experimental studies, most of them conducted on large and ultra large containership and a few of them on barges and ore carrier, conducted to investigate the high frequency vibrations, i.e. springing and whipping. All of these studies have revealed that the high frequency vibrations generally result in 30–40% increase in the extreme sagging load experienced by the ship.

Since the pioneering work of Bishop and Price (1977, 1979), significant developments have been achieved in the methods to calculate the hydroelastic loads acting on ships. They proposed method to couple the structural deformation of the hull with the hydrodynamic forces calculated using linear strip theory. Wu et al.

* Corresponding author.
E-mail address: c.guedes.soares@centec.tecnico.ulisboa.pt (C. Guedes Soares).

http://dx.doi.org/10.1016/j.oceaneng.2016.06.039
0029-8018/

(1991) extended the unified theory for calculation of hydroelastic response of slender bodies. Several other forms of strip theory had been proposed driven by the need to include the hydrodynamic forces acting in the ship's longitudinal direction which facilitated improvement in the calculation of flexible response of the hull using 3D FEM methods, Keane et al. (1991), Wang et al. (1991), Che et al. (1994) and Hirdaris et al. (2003).

The linear theories provided reasonable results for engineering applications in low to moderate seas. However in extreme seas, ship response becomes highly nonlinear, and in order to deal the problem, nonlinear hydroelastic theories were proposed. Yamamoto et al. (1980) presented a nonlinear hydroelastic method in which the hydrodynamic forces were calculated for the instantaneous draft but for a representative frequency. Jensen and Pedersen (1979) proposed a nonlinear quadratic strip theory, and later on extended the theory for accurate estimation of the springing response, Jensen and Pedersen (1981). Gu et al. (1988, 1989) introduced a 2D nonlinear model based on generalized strip theory. The radiation solution was presented by a time convolution method and the nonlinear hydrostatic forces and the momentum slamming forces were included. The hydrodynamic model was coupled with a Timoshenko model. Xia et al. (1998) proposed nonlinear hydroelastic theory based on strip theory. The memory functions due to the free surface effect were represented using higher order differential equation, and the body nonlinear hydrodynamic wave excitation forces and slamming forces were calculated. The method was used to calculate the vertical response of a S175 containership and the agreement with the experimental results was found to be good, particularly for low speed. Wu and Moan (1996) presented a nonlinear hydroelastic method where the linear part is evaluated using a linear strip theory and the nonlinear modification is obtained as the convolution of the linear impulse function and the nonlinear modification force.

Fonseca et al. (2006) presented a decoupled analysis using 2D nonlinear theory where the rigid body motions were calculated first using a partially nonlinear time domain method (Fonseca and Guedes Soares, 1998) and the hull vibration problem was solved in the next step, which is a similar approach as in Guedes Soares (1989), except that in that case a linear strip theory was used. The vertical bending moment (VBM) from the numerical method was compared with the experimental results for a frigate. Mikami and Kashiwagi (2008) derived a nonlinear hydroelasticity method based on strip theory for the calculation of the hull vibratory response in large amplitude waves. Body nonlinear hydrostatic and Froude–Krylov forces were included and the radiation force was represented by memory function and infinite frequency added mass. Similarly, in order to examine the behavior of the non-beam like structures 3D linear (Wu, 1984; Price and Wu, 1985), and nonlinear methods (Wu et al., 1997) have been proposed. Wu and Cui (2009) presented the detailed overview of the existing 3D linear and nonlinear methods for calculation of the hydroelastic response of the ships.

Ships hydroelastic response is more pronounced the more flexible ships are, which tend to increase with ship length for a given type of cross section. Santos et al. (2009a, 2009b) have applied hydroelastic theory to a small patrol boat to determine the limits of applicability of this type of approach. More recent developments in the numerical method proposed in the field of hydroelasticity are briefly reviewed in ISSC (2012).

The extreme motions and loads experienced by a ship during its life time are of prime importance during the structural designing of the ship. The capability of the linear methods to calculate the extreme response experienced by ships is inadequate and the nonlinear methods are highly preferred. Advanced 3D nonlinear methods based on the hydroelastic coupling between the 3D boundary element method and 3D FEM techniques give accurate results. However, their applicability for practical engineering application, at the least in the preliminary design stage, is still questionable due to heavy computations involved and large time consumption. Design vertical bending moment is generally estimated from the long term distribution of the loads in extreme sea conditions and various approaches have been proposed to combine wave frequency loads with other load components (Guedes Soares, 1992), including vibratory ones (Teixeira et al. 2013; Corak et al. 2015a, 2015b, Shi et al., 2016). Generally, probabilistic models are fitted to a 3 h short term distribution data in extreme sea conditions and are extrapolated to vessels life span. Ship responses in large amplitude waves and extreme sea conditions are highly nonlinear, which results mainly from the nonlinearity associated with free surface and geometry of ships.

While the work described deals with hydroelastic response of the ship hulls, the slamming loads are calculated without consideration of the hydroelastic response of local structures, although some work is available on this subject (e.g Faltinsen, 2000; Wang et al., 2016).

From the previous studies conducted by the authors, Rajendran et al. (2015a, 2016), it was clearly observed that the body nonlinear radiation forces, which is associated with the geometry of ships, plays a significant role in the estimation of the vertical bending moment at amidship for ships with large bow flare angle, like containerships. To the best knowledge of the authors, no studies have been conducted so far to analyze the hydroelastic response in irregular seas by taking account of the geometrical dependency of the radiation forces. Even though, the present study is restricted to large amplitude regular waves, it can be ascertained without any doubt that the body nonlinear method discussed in this paper can be easily extended for calculation of hydroelastic responses in irregular seas for producing response time series of long duration. Such an approach will be highly useful for estimation of the design vertical bending moment from the short term distribution of loads.

Two dimensional (2D) methods based on strip theory are faster and easier to implement and can calculate the short term distribution of the loads with acceptable accuracy for practical engineering application. Strip theory is a slow speed theory; however this restriction does not pose any problem in employing the theory for the calculation of ship responses in large amplitude waves and extreme seas, because the ships generally travels in extreme sea conditions with low speed. Strip theory being a linear theory, the nonlinearity of the ship responses in extreme conditions is dealt by means of time domain approaches. It is assumed that the pitch angles are small in extreme conditions; however relative motions between the ship and the wave may be of large amplitude leading to large variation of the immersed volume with associated nonlinear effects. This large immersion of the hull can be easily dealt with a time domain method.

Rajendran et al. (2013, 2014) improved the method proposed by Fonseca and Guedes Soares (1998) to calculate the vertical response of ships in extreme sea conditions using a body nonlinear time domain method based on strip theory. The authors calculated the rigid body response of a cruise vessel and an ULCS in large amplitude waves and extreme irregular seas using the time domain method. The hydrodynamic and hydrostatic forces were calculated at each time step taking account of the geometrical nonlinearity of the wetted hull. The radiation forces were represented by convolution of the memory functions. This method was further extended by Rajendran et al. (2015b), to analyze the hydroelastic load acting on an ULCS in severe head seas. Similar formulations are used in this paper for calculation of symmetric distortion of a large containership. However, the main objective of the paper is to numerically analyze the effect of hydroelasticity on the ship responses, which include both motions and loads, in large

amplitude waves using a body nonlinear method.

The containership was used for the recent ITTC-ISSC benchmark study in which the authors participated. The hull structural characteristics are represented by a Timoshenko beam and the global mass and stiffness matrix are calculated using the finite element method. The modal analysis is carried out to calculate the structural natural frequency and the modal matrix. The Froude-Krylov and the hydrostatic forces are calculated for the exact wetted surface area. The radiation forces are represented by means of the memory function and the memory functions are obtained from the Fourier transform of the hydrodynamic coefficient. The radiation and diffraction forces are also calculated for the exact wetted surface area following a practical engineering approach. The water entry and exit problems are modeled based on Von Karman method and the green water effect is calculated based on Buchner (1995) formulation.

2. Theory

Rajendran et al. (2015b) presented the theoretical formulation behind the body nonlinear time domain hydroelastic formulation. However, this is briefly presented here for the sake of completeness. A coordinate system fixed with respect to mean position of the ship is defined for the hydrodynamic problem. The origin is in the plane of the undisturbed free surface. Considering a ship advancing in waves and oscillating as an unrestrained rigid body, the oscillatory motions will consist of three translations and three rotations. The present work is restricted to head waves, thus the oscillatory motions to be studied are heave displacements and the pitch rotation.

2.1. Equation of motion

The equation of motion of a structure can be expressed as.

$$[M]\{\ddot{u}\} + [B]\{\dot{u}\} + [K]\{u\} = \{F(x,t)\} \tag{1}$$

where $[M]$ is the global mass matrix, $[B]$ is the global damping matrix and $[K]$ is the global stiffness matrix expressed in the physical coordinate. $[M]$ is a positive definite symmetric matrix and $[K]$ is a semi-definite symmetric matrix. $[M]$, $[K]$ and $[B]$ are calculated based on finite element formulation as discussed in the following section. $\{u\}$ is the nodal displacement vector and $\{F(x,t)\}$ is the structural distributed forces vector. According to the principle of modal superposition which is valid for linear responses, the distortion of structure can be expressed as a sum of the distortion in the principal modes.

$$u(x,y,z,t) = \sum_{r=0}^{m} \{u_r(x,y,z)\} p_r(t) = [D]\{p\} \tag{2}$$

where p_r is the principal coordinate, vector $u_r=(u_r, v_r, w_r)$ is the rth principal mode and $[D]$ is the modal matrix. Eq. (1) can be expressed as given below, in terms of the principal coordinates describing the dynamic response of a flexible structure.

$$\begin{aligned} &[m]\{\ddot{p}\} + [b]\{\dot{p}\} + [k]\{p\} = \{F_k(t)\} \\ &[m] = [D]^T[M][D], [b] = [D]^T[B][D], [k] \\ &\qquad = [D]^T[K][D], \{F_k(t)\} \\ &\qquad = [D]^T\{F_k(x,t)\} \end{aligned} \tag{3a-b}$$

where $[m]$, $[b]$ and $[k]$ are the generalized mass, damping and stiffness matrix of the dry structure. $\{F_k(t)\}$ is the generalized hydrodynamic force vector. Based on linear theory, the hydrodynamic forces are further divided into radiation, $\{F_k^R\}$, Froude–Krylov, $\{F_k^{FK}\}$, diffraction, $\{F_k^D\}$, and restoring forces, $\{F_k^H\}$, green water forces, $\{F_k^{GW}\}$, and slamming forces, $\{F_k^{slam}\}$.

$$\{F_k\} = \{F_k^R\} + \{F_k^{FK}\} + \{F_k^D\} + \{F_k^H\} + \{F_k^{GW}\} + \{F_k^{slam}\} \tag{4}$$

The radiation force can be written as:

$$\{F_k^R(t)\} = \sum_{r=1}^{N} \left(-[A_{kr}^{\infty}]\{\ddot{p}_r(t)\} - \int_0^t K_{kr}^m(t-\tau)\dot{p}_r(\tau)d\tau - [C_{kr}^m]\{p_r(t)\} \right), \quad k = 1, 2, \ldots N \tag{5}$$

where $[A_{kr}^{\infty}]$ is the infinite frequency added mass matrix which depend only on the ship geometry, and K_{kr}^m and $[C_{kr}^m]$ are the memory functions, and radiation restoration coefficients.

On substituting Eqs. (5) and (4) in (3a), the equation of motion in time domain for the flexible hull can be written as given in Eq. (6).

$$\begin{aligned} &\sum_{r=1}^{N} \left([m_{kr}] + [A_{kr}^{\infty}]\{\ddot{p}_r\} + [b_{kr}]\{\dot{p}_r\} \right. \\ &\qquad \left. + \int_0^t [K_{kr}^m(t-\tau)]\{\dot{p}_r(\tau)\}d\tau + ([C_{kr}^m] + [c_{kr}])\{p_r\} \right) \\ &= \{F_k^{FK}\} + \{F_k^D\} + \{F_k^H\} + \{F_k^{GW}\} + \{F_k^{slam}\}, \quad k = 1, 2, \ldots N \end{aligned} \tag{6}$$

where N is the maximum number of modes used for the calculation. m_{kr} and c_{kr} are diagonal matrix and b_{kr} is symmetric matrix. Finally the equation of motion is solved using finite difference method. Time stepping of the generalized coordinate can be written as

$$\begin{aligned} \{p_r\}^{t+1} = &\left(\frac{[m_{kr}]}{\Delta t^2} + \frac{[b_{kr}]}{2\Delta t} \right)^{-1} \\ &\left[\left(\frac{2([m_{kr}])}{\Delta t^2} - [c_{kr}] \right)\{p_r\}^t + \left(\frac{[b_{kr}]}{2\Delta t} - \frac{[m_{kr}]}{\Delta t^2} \right)\{p_r\}^{t-1} \right. \\ &\left. + \{F_k\}^t \right] \\ &k, r = 1, 2, \ldots N \end{aligned} \tag{7}$$

where superscript t shows the particular time instant and $t+1$ shows the next time instant and Δt is the increment in time. The initial calculation for the $t-1$ s can be done using following equation

$$\{p_r\}^{t-1} = \{p_r\}^0 - \Delta t\{\dot{p}_r\}^0 + \frac{\Delta t^2}{2}\{\ddot{p}_r\}^0 \tag{8}$$

Initial acceleration can be calculated using the following equation

$$\{\ddot{p}_r\}^0 = \frac{1}{([m_{kr}])}\left(\{F_k\}^0 - [b_{kr}]\{\dot{p}_r\}^0 - [c_{kr}]\{p_r\}^0 \right) \tag{9}$$

Superscript t and 0 shows the time instants and $\{F_k\}$ shows the generalized vectors of the hydrodynamic, hydrostatic and exciting (Froude–Krylov, diffraction, slamming, green water etc.) forces calculated for each time instant.

In order to converge, it is necessary that $\Delta t \le \frac{T_n}{\pi}$, where T_n is the natural period of the highest mode that is represented in the model. However, it is recommended that the time step should be 10 times lower than the natural period of the highest mode.

2.1.1. Radiation force

The radiation force is calculated using Eq. (5). For a 2D problem for the calculation of symmetric distortion in head waves, the principal mode vector, u_r, is replaced with its z component $w_r(x)$. The memory functions, K_{kr}^m and radiation restoration coefficients, $[C_{kr}^m]$ are calculated from the frequency dependent hydrodynamic

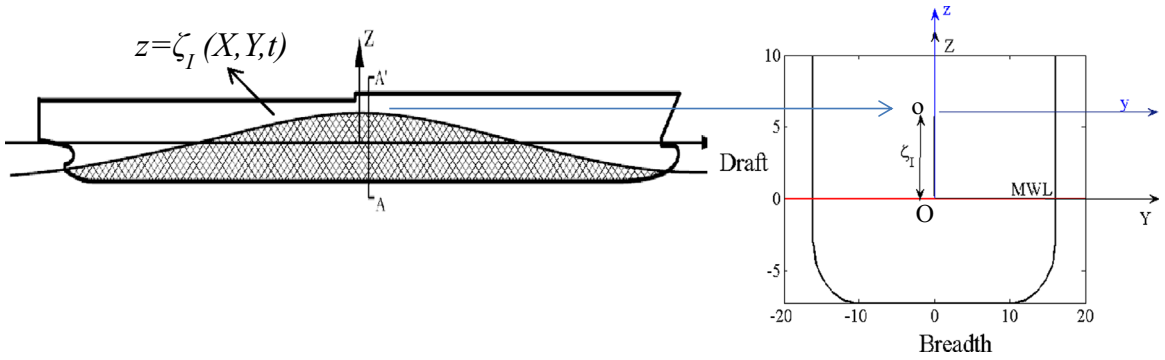

Fig. 1. Coordinate transformation between the original and new coordinate system.

coefficients using

$$\left[A_{kr}^{\infty}\right] = \int_0^l m^{\infty}(x) w_k(x) w_r(x) dx$$
$$\left[K_{kr}^{m}(t)\right] = \frac{2}{\pi}\int_0^{\infty}\left(B_{kr}(\omega)\cos(\omega t)\right)d\omega$$
$$\left[C_{kr}^{m}\right] = \omega^2\left[A_{kr}^{\infty} - A_{kr}(\omega)\right] - \omega\int_0^{\infty}\left(K_{kr}^{m}(\tau)\sin(\omega t)\right)d\tau \quad (10a\text{-}c)$$

where $w_r(x)$ is the upward vertical deflection in rth mode. Infinite frequency added mass for heave and pitch are calculated using the following given by Bishop and Price (1978)

$$m_{\infty} = \rho\pi a_0^2\left[(1+a_1)^2 + \sum_{n=1}^{N}(a_{2n-1})^2(2n+1)\right] \quad (11)$$

where $a_0 \ldots a_n$ are the conformal mapping coefficients, N is the mapping parameter and ρ is the density of the fluid. The frequency dependent added mass $\left[A_{kr}(\omega)\right]$, damping coefficients $\left[B_{kr}(\omega)\right]$ are calculated using the following equation

$$\left[A_{kr}(\omega)\right] = \int_0^l \left(\begin{array}{l} m(x)w_k(x)w_r(x) + \frac{U^2}{\omega^2}m(x)w'_k(x)w'_r(x) \\ + \frac{U}{\omega^2}N(x)\left[w_k(x)w'_r(x) - w'_k(x)w_r(x)\right]\end{array}\right)dx$$
$$- \frac{U^2}{\omega^2}\left[m(x)w_k(x)w'_r(x)\right]_0^l + \frac{U}{\omega^2}\left[m(x)w_k(x)w_r(x)\right]_0^l$$
$$\left[B_{kr}(\omega)\right] = \int_0^l \left(\begin{array}{l} N(x)w_k(x)w_r(x) + \frac{U^2}{\omega^2}N(x)w'_k(x)w'_r(x) \\ + Um(x)\left[w'_k(x)w_r(x) - w_k(x)w'_r(x)\right]\end{array}\right)dx$$
$$- \frac{U^2}{\omega^2}\left[N(x)w_k(x)w'_r(x)\right]_0^l - U\left[m(x)w_k(x)w_r(x)\right]_0^l \quad (12a, b)$$

where $m(x)$ and $N(x)$ are the sectional added mass and damping coefficient calculated using multi-parameter conformal mapping as given by Rajendran et al. (2015a). $w'_k(x)$ shows the spatial derivative of the upward deflection. Here the sectional added mass and damping are calculated for the instantaneous wetted surface area.

Rajendran et al. (2015a) proposed a simplified method for calculation of the body nonlinear radiation forces of a rigid body. Similar approach is also used in this paper. In large amplitude waves, the ship's wetted surface area changed drastically and hence it should be taken into account, not only for calculation of Froude–Krylov and hydrostatic forces but also for radiation/diffraction force. Since it is our objective to include the body nonlinearity in the calculation of time domain radiation/diffraction forces, Eq. (12) along with infinite frequency added mass is to be updated at each instant of time before substituting in Eq. (5), which is still a linear formulation derived after application of linear radiation boundary condition. So the current formulation would be rather considered as a practical engineering approach for purpose of easy implementation and accurate results.

A new local coordinate system was defined for the each ship section as shown Fig. 1, where *OYZ* is the original coordinate system located at the mean water level and *oyz* is the new coordinate system. For each time step, the new coordinate system, *oyz,* is defined at the intersection between the incident wave profile, $z=\zeta_I(X,Y,t)$, and the ship sections. The coordinate transformation between them could be written as $x = X$, $y = Y$, $z(t)=Z-\zeta_I(t)$ and $\Phi(X, Y, Z, t)$ and $\phi(x, y, z, t)$, respectively, are the velocity potential defined in the original and new coordinate system.

The linear free surface condition can be written as

$$\frac{\partial^2\Phi}{\partial t^2} + g\frac{\partial\Phi}{\partial Z} = 0$$
$$\frac{\partial\Phi}{\partial t} = \frac{\partial\phi}{\partial t} + \frac{\partial\phi}{\partial z}\frac{\partial z}{\partial t} = \frac{\partial\phi}{\partial t} - \frac{\partial\phi}{\partial z}\dot{\zeta}_I$$
$$\frac{\partial^2\Phi}{\partial t^2} = \frac{\partial}{\partial t}\left(\frac{\partial\phi}{\partial t} - \frac{\partial\phi}{\partial z}\dot{\zeta}_I\right) + \frac{\partial z}{\partial t}\frac{\partial}{\partial z}\left(\frac{\partial\phi}{\partial t} - \frac{\partial\phi}{\partial z}\dot{\zeta}_I\right)$$
$$= \frac{\partial^2\phi}{\partial t^2} - 2\frac{\partial^2\phi}{\partial t\partial z}\dot{\zeta}_I - \frac{\partial\phi}{\partial z}\ddot{\zeta}_I + \frac{\partial^2\phi}{\partial z^2}\dot{\zeta}_I^2$$
$$\frac{\partial^2\phi}{\partial t^2} - 2\frac{\partial^2\phi}{\partial t\partial z}\dot{\zeta}_I - \frac{\partial\phi}{\partial z}\ddot{\zeta}_I + \frac{\partial^2\phi}{\partial z^2}\dot{\zeta}_I^2 + g\frac{\partial\Phi}{\partial z} = 0 \quad (13)$$

Based on weak scattering and small amplitude incident waves, the terms involving ζ_I are neglected and finally, the linear free surface condition is rewritten in the new coordinate system as

$$\frac{\partial^2\phi}{\partial t^2} + g\frac{\partial\Phi}{\partial z} = 0 \quad (14)$$

The linearized body boundary conditions do not change as they do not involve any time derivative. The boundary conditions are still linear; however the method is useful for calculation of the linear time dependent hydrodynamic forces. Following procedures have been adopted in the numerical calculation for calculation of body nonlinear radiation force.

1. In the pre-processing stage, the sectional added mass, damping coefficients and infinite frequency added mass are calculated for a range of drafts.
2. During the time domain calculation, the sectional added mass, damping coefficient and infinite frequency added mass which correspond to the exact draft of the section, which includes total the vertical deflection of the section as given by Eq. (15), from the undisturbed incident wave profile is calculated for each time step through interpolation of the aforementioned pre-calculated data.
3. At each time step, the interpolated values of the sectional coefficients are substituted in Eq. (12) to obtain the global hydrodynamic coefficients. The new global hydrodynamic coefficients are substituted in Eq. (10) to obtain the memory function and the hydrodynamic restoring coefficients of the ship calculated for the exact wetted surface. Similarly, sectional infinite frequency added mass is substituted in Eq. (11) for

calculating the global infinite frequency added mass corresponding to the exact wetted surface area under the undisturbed incident wave profile.

The exact draft of a point on a section from the undisturbed incident wave elevation is calculated using the following equation.

$$z_d = Z + \sum_{r=0}^{m} \{ w_r(x) \} p_r(t) - \eta(x, t) \tag{15}$$

where Z is the vertical coordinate of a point on the ship surface in the equilibrium position defined with respect to the mean water level, η is the incident wave elevation, and z_d is the submerged depth of a point from the incident wave profile calculated for each time step.

2.1.2. Diffraction force

The diffraction force for the head sea condition can be calculated using the Eq. (16) as shown in Bishop and Price (1979). Here again, the sectional added mass and damping are updated during each time step according to the exact wetted surface.

$$\left\{ F_k^D(t) \right\} = \mathrm{Re}\left[\zeta_a e^{i(\omega_e t + \theta_k)} \left(-\omega_0 e^{kz} e^{ikx} \int_L \left\{ \begin{array}{l} \frac{\omega_0}{\omega_e}(\omega_e m(x) - iN(x)) w_k dx + \\ \frac{U}{i\omega_e} e^{ikx+kz}(\omega_e m(x) - iN(x)) w'_k \, dx \end{array} \right\} \right) \right] - \left[\omega_0 \frac{U}{i\omega_e} e^{ikx*+kz}(\omega_e m(x) - iN(x)) w_k \right]_0^l \tag{16}$$

where ω and ω_e are the incident wave frequency and encounter frequency and z is the vertical distance between the centroid of the underwater section and the frame of reference.

2.1.3. Froude–Krylov and hydrostatic force

The Froude–Krylov force, F_k^{FK}, in head seas is calculated using the following equation.

$$\left\{ F_k^{FK}(t) \right\} = \mathrm{Re}\left[\rho g \zeta_a e^{i(\omega_e t + \theta)} \int_{L*} \int_{Cx} n_z e^{ikx+kz} w_k(x) dl dx \right] \tag{17}$$

where ζ_a is the incident wave amplitude and integration is over the wetted cross section contour, C_x under the incident wave elevation, n_z is the unit vector normal to the wetted surface in the z-direction, ρ represents the density of the fluid, g is the gravity acceleration and k is the wave number, dl is the incremental length along the girth of ship section and 'z' is the exact draft of a point on the ship surface is given by $z = Z + \sum_{r=0}^{m} w_r(x) p_r(t)$, where Z is the vertical coordinate of a point on the ship surface in equilibrium position defined with respect to the mean water level. Pressure between the mean water line and the wave crest is assumed to be hydrostatic.

The hydrostatic forces $F^H$is calculated using the following equation

$$\left\{ F_k^H(t) \right\} = -\rho g \int_L \int_{Cx} n_z \; z \, w_k(x) dl \, dx - \left\{ F_{Static}^H \right\} \tag{18}$$

where F_{Static}^H is the static equilibrium hydrostatic force. The hydrostatic force is calculated for the 'exact' wetted surface.

2.1.4. Slamming force

Based on Von-Karman model where the water pile up is assumed to be zero, slamming force is calculated based on 'momentum' equations

$$\left\{ F_k^{slam}(t) \right\} = \int_L f^{slam} w_k(x) dx$$

$$f^{slam} = \frac{\partial m(x)}{\partial t} \frac{Dw_{rel}}{Dt} - U \frac{\partial m(x)}{\partial x} \frac{Dw_{rel}}{Dt} \tag{19}$$

The second term is neglected assuming that the ship is slender and the variation of the added mass in the longitudinal direction is negligible A comparison between this formulation and others can be found in Wang and Guedes Soares (2013, 2014a, 2014b). The material derivative of the relative motion is given by.

$$\frac{Dw_{rel}}{Dt} = \sum_{r=0}^{m} w_r(x) \frac{\partial p_r(t)}{\partial t} - U \sum_{r=0}^{m} p_r(t) \frac{\partial w_r(x)}{\partial x} - \mathrm{Re}\left(i\zeta_a \omega e^{i(\omega_e t + \theta_k)} e^{ikx+kz} \right) \tag{20}$$

2.1.5. Green water force

Vertical forces acting on the deck during the presence of green water is calculated using the momentum method (Buchner, 1995).

The vertical force per unit length due to presence of green water is given by:

$$\left\{ F_k^{GW}(t) \right\} = \int_L F^{gw} w_k(x) dx$$

$$F^{gw}(x, t) = \left(\frac{\partial m_{gw}}{dt} \right) w + \left(g \cos \xi_5 + \frac{\partial w}{dt} \right) m_{gw} \tag{21}$$

The first term on the right hand side denotes the rate of change of mass of water over the deck. The mass of water on deck is calculated from the height of water above the deck which is obtained from the vertical distance between the relative motion and freeboard. The second term denotes the hydrostatic component and the third term denotes the acceleration of the deck. 'w' is the velocity of deck. The performance of this approach can be assessed from the results of Fonseca and Guedes Soares (2005).

2.1.6. Finite element model (FEM)

The global mass and stiffness matrix are calculated from the finite element analysis (Rajendran et al., 2015a, 2015b). The ship hull is represented by a non-uniform Timoshenko beam which can take account of the shear deformation. Structural natural frequency is calculated using the modal analysis. The mass and stiffness matrix is derived from the kinetic and potential energy formulation, respectively, which takes account of the deflection and rotation of the beam. The modal matrix given in 2(2), each column of which represents the principal modes, is estimated from the Eigen value calculation of the undamped free vibration. The eigen vectors represent the mode shape and the eigen values represent the natural frequencies. The structural damping is taken as 2% of the critical damping as calculated during the experiment.

3. Results

The numerical results have been obtained as required to compare with the available experimental results. This section describes thus the experimental set up and then the numerical results.

3.1. Experimental set up

A scaled model (1:70) of a Container Ship was constructed in FRP. In order to reproduce the effect of the deformation modes on the loads, the model has the same scaled flexible characteristics of the real ship. This was achieved by dividing the model in eight segments and joining it with an aluminum backbone of variable structural characteristics along the hull. This beam was fitted with strain gauges to measure the forces and moments transmitted at each cut.

Fig. 2 shows the body plan of the containership and Fig. 3 shows the weight distribution along the length of the ship. The model used for testing in the wave basin is shown in Fig. 4. The main particulars of the ship are given in Table 1. The tests were carried out in small amplitude regular waves for the estimation of the vertical response RAOs. The ship response in moderate to large amplitude was calculated by testing the model in three sets of regular waves. Table 2 gives the position of the strain gauges from the aft perpendicular (full scale measurement) and Table 3 gives the details of the regular waves. The tests were carried out for 5 and 12 knots (Froude number $=0.05$ and 0.12).

3.2. Wet natural frequency and modes

The numerically calculated first five wet natural modes of vertical vibration, represented by Eigen vectors of the undamped free vibration of the structure, are shown in Fig. 5. The normalized values of the modes are plotted against the length of the ship, which is normalized by the length between perpendiculars (L_{PP}). 0 and 1 on the x-axis show the aft and forward perpendicular. The modes are normalized by dividing with $w_r(0)$, rth principal mode value at the aft. The first two modes that represent the rigid body motion i.e. heave and pitch respectively, and the first three flexible modes are presented. Table 4 compares the measured first wet natural frequency of the model with the numerical one. The calculated eigenvalues of the undamped free vibrating system, which represent the natural frequency, are in good agreement with the experimental value.

3.3. Vertical response RAOs

The numerical and the experimental linear transfer functions of the vertical motions and the bending moment at the cut4 are given in Fig. 6. The given responses are for zero Froude number. The responses are measured in small amplitude waves and the numerical response amplitude operators (RAOs) are calculated from the time domain results in small amplitude regular waves. The pitch RAOs are divided by the wave number (k) and the VBM (M_5) by the density (ρ), acceleration due to gravity (g), square of the length between perpendiculars (L_{pp}), breadth of the ship (B) and wave amplitude (ζ_a) in order to make them non-dimensional.

One can observe that the numerical heave RAOs are able to follow the measured ones except for wavelengths close to ship length for which the ship experiences the largest relative motion. For the zero speed, the strip theory gives good results for the pure vertical motion (heave into heave) hydrodynamics (Fonseca and Guedes Soares., 2004). However, the coupled pitch into heave damping coefficients are generally overestimated by the theory, which probably leads to the underestimation of the heave response.

The pitch RAOs are better predicted by the numerical model, however they slightly overestimate where the largest relative motion occurs. This is probably due to the role played by the viscous damping in pitch motion. Even though the ship has small pitch angle, the ship motion in waves with length close to the ship length will result in considerable pitch velocity and associated viscous damping, which is neglected in the potential code. Beukelman (1983) showed that, like the roll motion, the vertical motion is also affected by the viscous effect due to flow separation. The results suggested that the drag coefficient is a function of the frequency, which implies that the free surface wave influence the vortex shedding. Therefore, separation of the flow and the associated energy dissipation under the flat bottom and the bow flare region, which is not considered in the potential flow method, can be a probable reason behind the discrepancy in the numerical and experimental results and needs to be further investigated. Similarly, the numerical VBM RAOs are in good agreement with the experimental ones except at the peak of the curve, where the

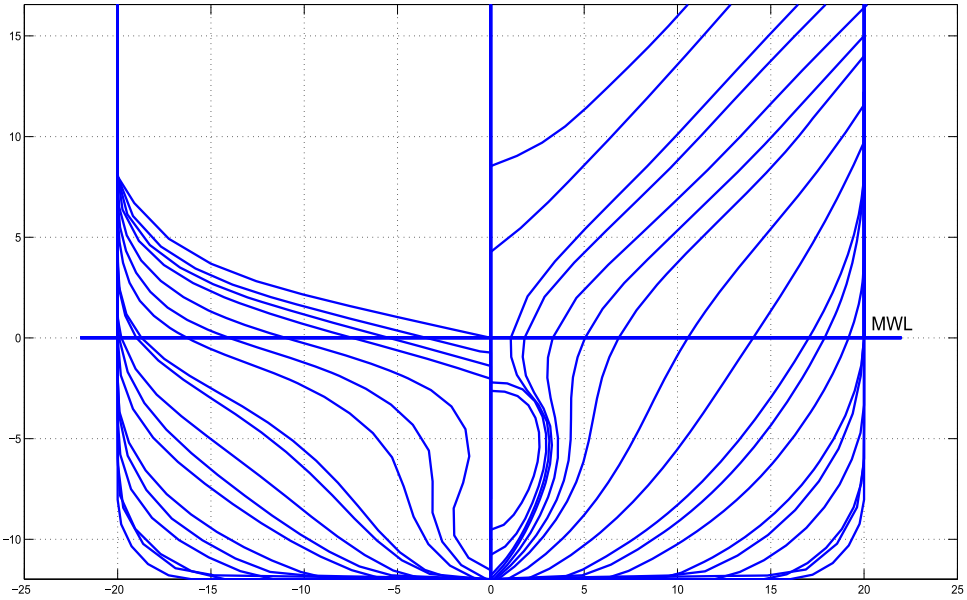

Fig. 2. Body plan of the containership.

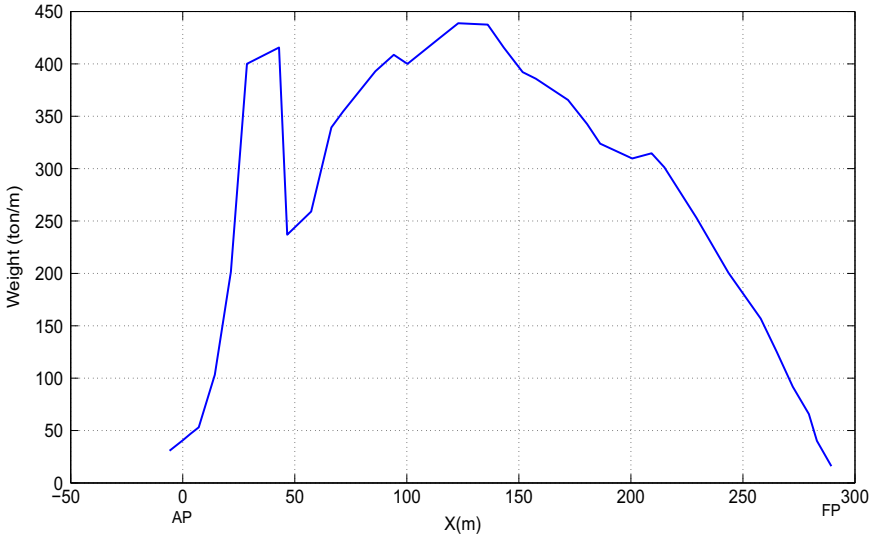

Fig. 3. Weight distribution of the containership.

numerical model overestimates the VBM at cut4. The VBM at the midship depends on the relative motion at the bow. Therefore larger pitch motion of the numerical model results in larger relative motion at the bow, which leads to an increase in the VBM in the numerical simulation.

3.4. Time series comparison

The numerical and the measured time series of the non-dimensional heave, pitch values at the mass center and the vertical bending moment at cut 4 are shown in Fig. 7. The experiments, represented by the dotted line, were conducted in regular waves with a wave to ship length of 1.06. Table 3 shows the details of the regular waves used for the simulations. Numerical simulations are represented by the solid line. The heave motions are underestimated by the numerical method and the pitch motions are slightly overestimated, as observed in Fig. 7. The high frequency vibrations are clearly observed for the vertical bending moment for the second case where the ship encounters large amplitude waves of 10.93 m wave height. The comparison between the numerical and the experimental results are quite satisfactory, particularly for the vertical bending moment. The higher order harmonics of the vertical responses are extracted by means of Fast Fourier Transforms and are further analyzed in the following section.

3.5. First and higher order harmonics in large amplitude waves

Fig. 8 compare the harmonics of the numerical and the experimental heave and pitch motion. The stems with circular and square head show the experimental and the numerical results, respectively. Regarding the experimental results, the hydro-

Table 1
Main particulars of the Containership.

Item	Prototype
Scale of the model	1/70
LOA (m)	300.9
LBP (m)	286.6
Breadth (m)	40
Depth (m)	24.2
Draft (m)	11.98
Displacement(ton)	85562.7
KG (m)	16.562
LCG from AP (m)	138.395
Radius of Gyration about x-axis, k_{xx} (m)	14.4
Radius of Gyration about y-axis, k_{yy} (m)	70.144
Radius of Gyration about z-axis, k_{zz} (m)	70.144
Neutral axis from keel (m)	11.412

Table 2
Location of the strain gauges from AP (m)-Full scale.

Cut1	Cut2	Cut3	Cut4	Cut5	Cut6	Cut 7
46.64	66.34	94.21	122.97	151.73	180.5	209.3

Table 3
Details of the experimental regular waves (full scale).

No	H (m)	λ/Lpp	Froude number
Case 1	6.118	1.06	0.05
Case 2	10.926	1.06	0.05
Case 3	6.118	1.06	0.12

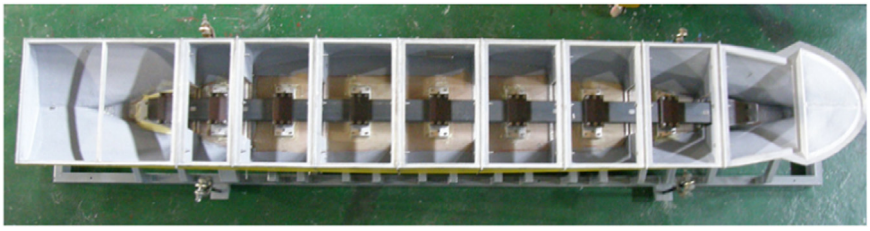

Fig. 4. Model used for testing in the wave basin.

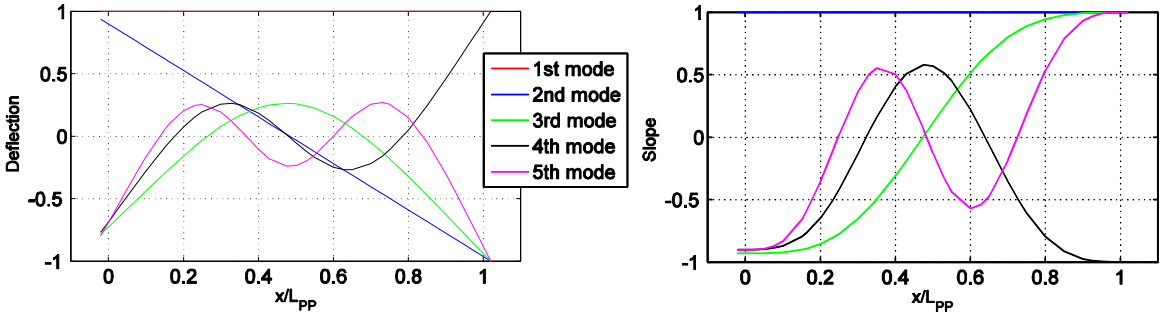

Fig. 5. Wet natural frequency modes of the numerical hull.

Table 4
Full scale natural vertical bending frequencies (Hz).

No	Wet (Exp)	Wet (Num)
1st mode	0.645	0.64
2nd mode	–	1.64
3rd mode	–	3.11

elasticity has little effect on the vertical motion and the 2nd order harmonic value is less than 10% of the first harmonics for the analyzed cases. The speed of the vessel significantly influences the first harmonics of the heave motion and it increases by 31% when the speed of the model is increased by 140%. However, the wave steepness has little effect on the first harmonics and the response is almost linear even in large amplitude waves for low Froude number. The geometrical nonlinearity associated with the bow and stern of the ship becomes less dominant due to the presence of the large parallel middle body of the ship which should have resulted in a linear vertical motion. The numerical results qualitatively follow the measured vertical motions; however its first harmonic values are smaller and larger, respectively, than the experimental heave and pitch values. This is also observed in Fig. 6 where the RAOs are compared for which the discussion has been held in Section 3.3.

Fig. 9 compares the magnitudes of the amplitude spectra of the numerical and the experimental VBM harmonics at cut 4. The first wet natural frequency of the structure occurs at 4.05 rad/s and the tests were conducted in regular waves with 0.45 rad/s. Therefore, it is expected that for the case 1 and 2 for which the ship moves with a Froude number of 0.05, 8th harmonics of the vertical bending moment will be amplified. Similarly, for the third case where the ship has a Froude number of 0.12, the 7th harmonics will be amplified as a result of the nonlinear springing. For none of the cases, the numerical model undergoes slamming. Unlike the vertical motions, the VBM at the cut4 is nonlinear due to the significant contribution from the geometrical nonlinearity associated with the bow of the ship. It is well known that the FD strip theory has a tendency to overestimate ship responses (first order harmonics), which is also observed in this paper for the first

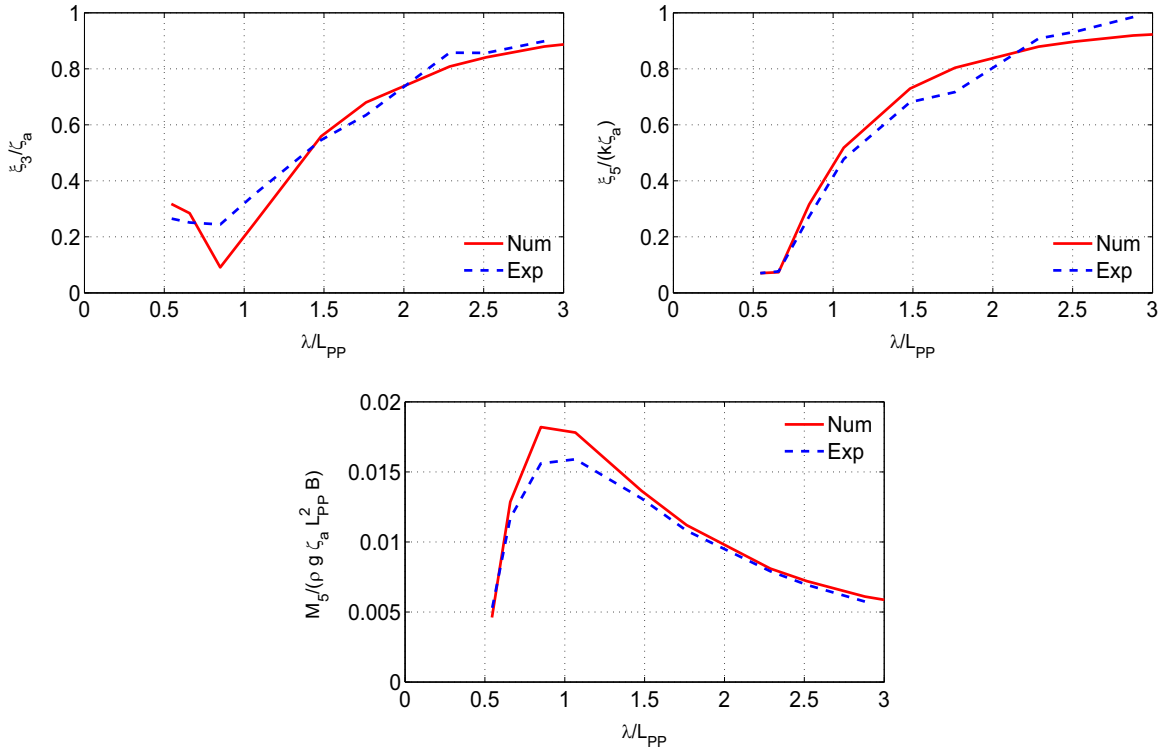

Fig. 6. The experimental and numerical heave, pitch and vertical bending moment RAOs.

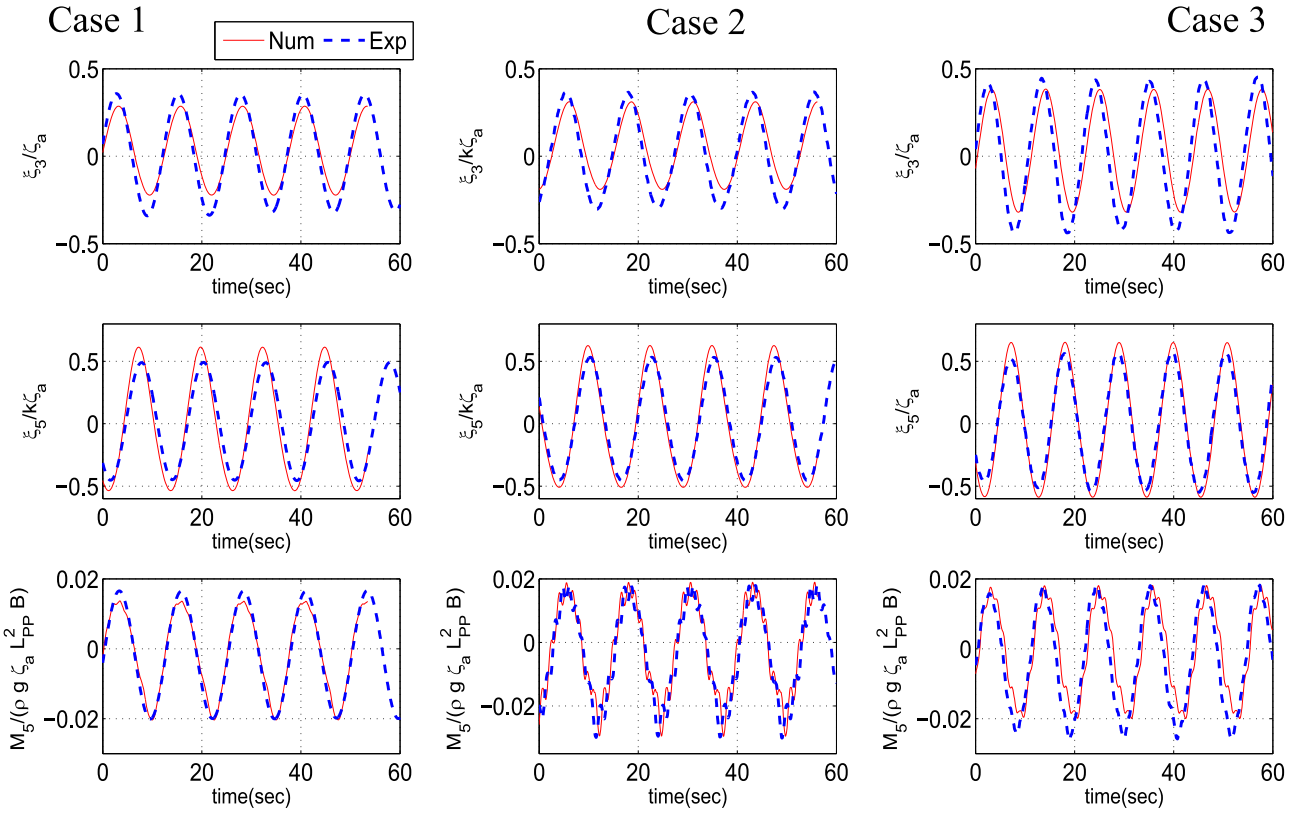

Fig. 7. Time series comparison of the numerical and the experimental heave, pitch and the vertical bending moment at cut 4.

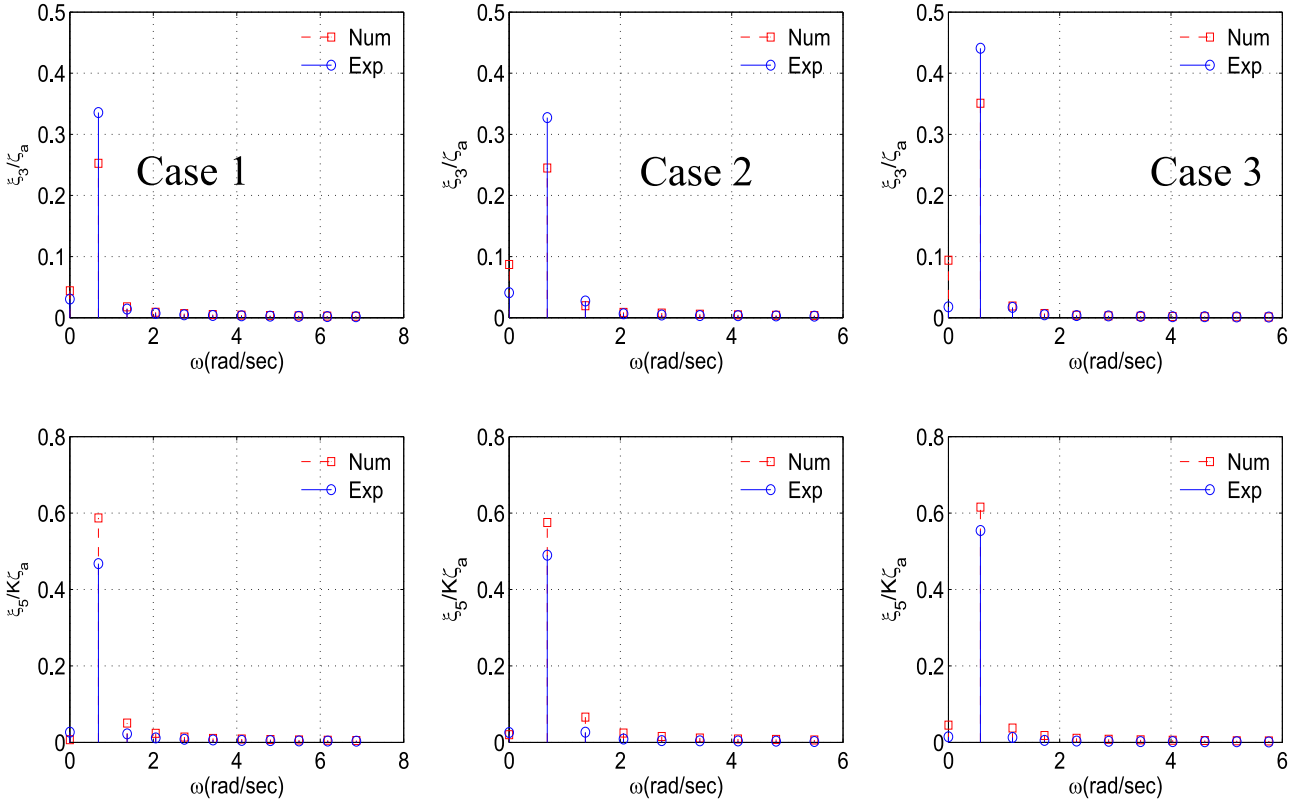

Fig. 8. The experimental and numerical amplitude spectra for the heave and pitch.

harmonics of pitch and vertical bending moment. Even though, the motions are little affected by nonlinearities, the loads are very much influenced by them. The time domain method is able to capture the nonlinearities associated with the geometrical non-linearity. The nonlinearities associated with bow flare strongly influences the vertical bending moment at midship, while the long

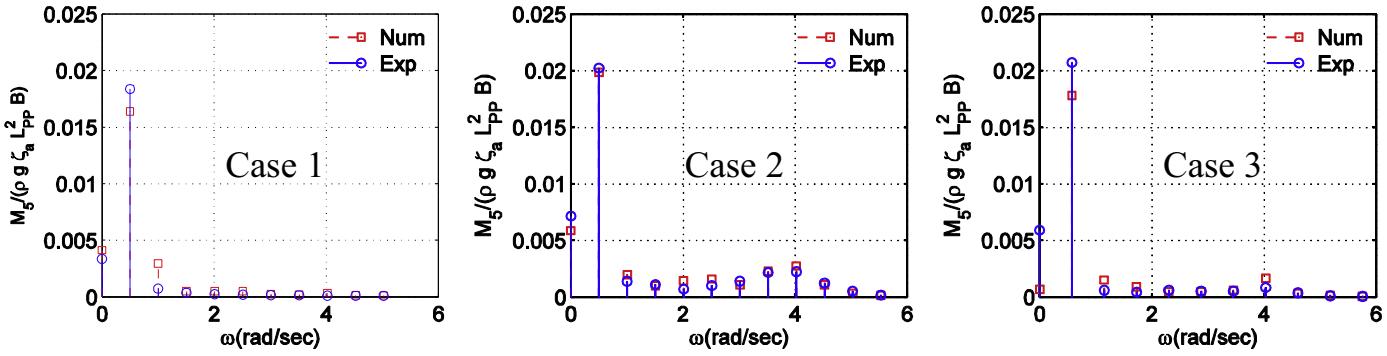

Fig. 9. The experimental and numerical amplitude spectra for the vertical bending moment.

parallel middle body of the ship plays a major role in the estimation of the motions which nullifies the nonlinearities associated with the bow flare.

On comparison of the experimental VBM linear transfer function in small amplitude waves given in Fig. 6, it is observed that the first order harmonic values are dependent on the wave steepness and the Froude number. The 1st order harmonic values increase by 15% and 27%, respectively, for case 1 and 2 and by 30% for case 3, for which the ship moves with higher Froude number. The experimental results in moderate to large amplitude regular waves, 1, 2 and 3, show that 80% increase in the wave amplitude results only in a 10% increase in the first harmonics and 140% increase in the Froude number results in 12% increase. In general, one can observe that the wave steepness and the Froude number significantly influence the first harmonics of VBM only up to moderate seas.

Except for the 2nd case, the higher order harmonics values are always less than 10% of the first harmonics. For the 2nd case, in which ship encounters the largest wave, 7th and 8th harmonic values are 10 and 11%, respectively, of the first order harmonics. It is observed that the higher order harmonics increases as the wave severity increases. Table 5 shows the percentage of variation of the experimental VBM harmonics with respect to the wave steepness and Froude number. The 8th harmonic, which lies in the vicinity of first wet natural frequency of beam, increases by 20 times when the wave steepness is increased by 80%. The mean values, which mainly results from the steady effect due to the forward speed of the ship and the wave effects, contribute significantly to total VBM. However, for case 1 and 2, the contribution from the steady effects should be negligible as the ship moves with a low Froude number and they contribute up to 18 and 35% of the first harmonics. The mean values are negative which shows the mean sagging value.

Regarding the numerical results, the results are fairly in good agreement with the experimental ones. Unlike the VBM RAO observed in Fig. 6, where the numerical results were larger than the measured ones, here the first harmonics of the numerical VBM is smaller for the case 1 and 3. From small to moderate waves, the first harmonic value decreases as the wave steepness increases, however from moderate to large amplitude wave, its value increases with the wave steepness. It is observed that the wave steepness has little effect on the heave and pitch motion, therefore its influence on the VBM at cut4 should be coming from the geometrical nonlinearity of the bow of the ship which plays a significant role in the estimation of the VBM close to the midship. However, it is difficult to explain the exact reason on the behavior of the first order harmonics on wave steepness. The numerically calculated higher order harmonics in large amplitude waves are in very good agreement with the experimental ones. The springing

Table 5
Influence of wave steepness and Froude number on the VBM harmonics.

Order of the Harmonics	$\frac{VBM^{(2)}-VBM^{(1)}}{VBM^{(1)}}$	$\frac{VBM^{(3)}-VBM^{(1)}}{VBM^{(1)}}$
0th	1.1	0.7
1st	0.1	0.1
2nd	0.9	−0.2
3rd	2.1	0.2
4th	1.9	1.5
5th	4.5	1.9
6th	8.1	2.5
7th	15.8	5.5
8th	19.0	2.3
9th	11.5	0.1
10th	5.2	−0.2

effect is very well represented by the numerical model in large amplitude waves and the model is able to capture the hydroelastic effect.

Finally the non-dimensional VBM peak along the length of ship is plotted for the test cases 1, 2 and 3 in Fig. 10. Zero denotes the aft perpendicular and one shows the Forward perpendicular. The agreement between the numerical and the experimental results are satisfactory. The numerical methods slightly overestimate the sagging peaks at the stern of the ship and slightly underestimate at the bow. A probable reason is the difference in the numerical and the experimental hull characteristics at the both end of the ships. Since there was no mode shapes available from the experimental set up for comparison, it will be difficult to come to a conclusion.

4. Conclusion

This paper deals with the numerical analysis of the hydroelastic response of a containership and its comparison with experimental results. The ship was tested in moderate to large amplitude regular waves for the frequency for which the ship experiences the largest relative motion. A 2D body nonlinear method based on strip theory is used to calculate the ship responses and the hull characteristics are modeled using a Timoshenko beam. The numerical model gives a good estimation for the first wet natural frequency of vertical vibration. The vertical response RAOs in small amplitude regular waves shows slight discrepancy between the numerical and experimental results at the peak of the curve. The time series comparison in moderate to large amplitude waves show similar trends for the first harmonic values, however the model is able to capture the hydroelastic effect and represent the

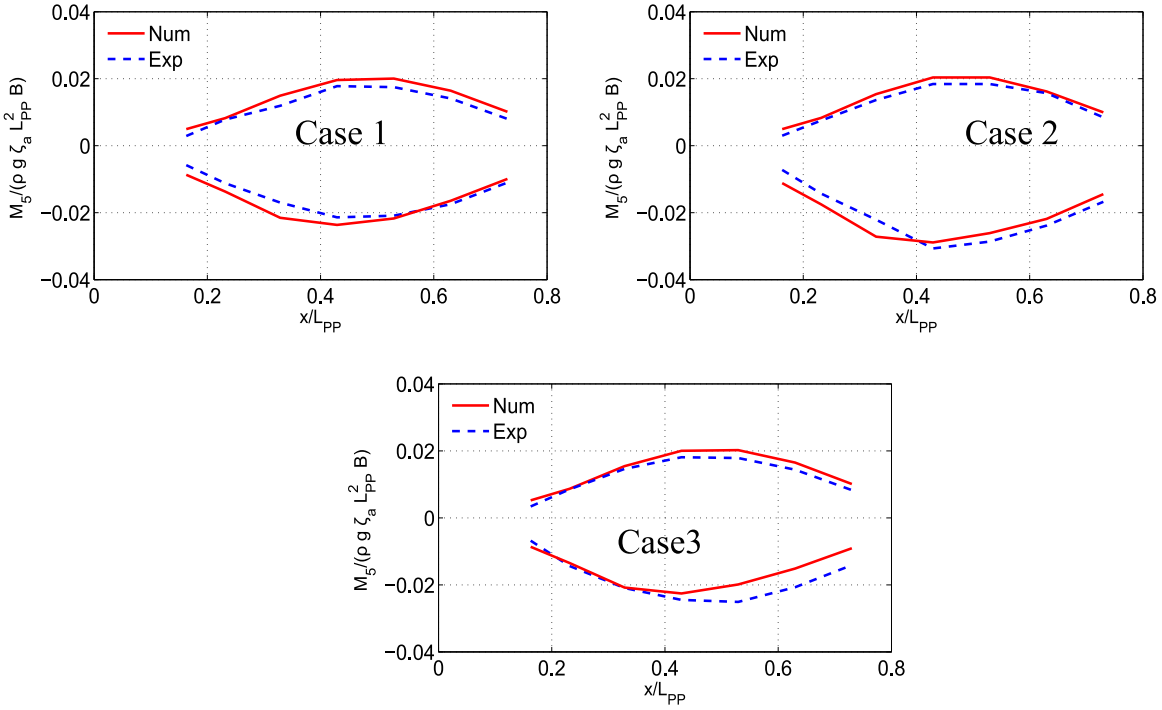

Fig. 10. The experimental and numerical amplitude spectra for the vertical bending moment along the length of the ship.

nonlinear springing very well. Springing has little effect on the vertical motions; however it significantly influences the VBM. The higher order harmonics of VBM at cut4 increase as the wave steepness increase and its influence on the harmonics lying close to the first wet natural frequency is found to be largest.

Acknowledgment

This work has been done in the scope of the benchmark study that was the basis for the 2014 ITTC-ISSC workshop. the experimental work was made available to participants and DAEWOO is to be thanked for having made the data available. This work was performed within the strategic research plan of the center for marine technology and ocean engineering, which is financed by Portuguese Foundation for Science and Technology (Fundação para a Ciência e Tecnologia – FCT).

References

Beukelman, W., 1983. Vertical Motions and Added Resistance of a Rectangular and Triangular Cylinder in Waves, Report No.510. Ship Hydrodynamics Laboratory, Delft University of Technology, the Netherlands.

Bishop, R.E.D., Price, W.G., 1977. The generalized antisymmetric fluid forces applied to a ship in a seaway. Int. Shipbuild. Progress 24, 3–14.

Bishop, R.E.D., Price, W.G., 1978. Hydrodynamic coefficients of some heaving cylinders of arbitrary shape. Int. J. Numer. Methods Eng. 13, 17–33.

Bishop, R.E.D., Price, W.G., 1979. Hydroelasticity of Ships. Cambridge University Press.

Buchner, B., 1995. The impact of green water on FPSO design. Offshore Technology Conference. pp. 45–47.

Che, X.L., Riggs, H.R., Ertekin, R.C., 1994. Composite 2D/3D hydroelastic-analysis method for floating structures. J. Eng. Mech. 120 (7), 1499–1518.

Corak, M., Parunov, J., Guedes Soares, C., 2015a. Long-term prediction of combined wave and whipping bending moments of containership. Ship Offshore Struct. 10 (1), 4–19.

Corak, M., Parunov, J., Guedes Soares, C., 2015b. Probabilistic load combination factors of wave and whipping bending moments. J. Ship Res. 59 (1), 11–30.

Drummen, I., Holtmann, M., 2014. Benchmark study of slamming and whipping. Ocean Eng. 86, 3–10.

Faltinsen, O.M., 2000. Hydroelastic slamming. Mar. Struct. 16, 175–182.

Fonseca, N., Guedes Soares, C., 1998. Time-domain analysis of large-amplitude vertical ship motions and wave loads. J. Ship Res. 42 (2), 139–153.

Fonseca, N., Guedes Soares, C., 2004. Validation of a time-domain strip method to calculate the motions and loads on a fast monohull. Appl. Ocean Res. 26, 256–273.

Fonseca, N., Guedes Soares, C., 2005. Experimental investigation of the shipping of water on the bow of a containership. J. Offshore Mech. Arct. Eng. 127 (4), 322–330.

Fonseca, N., Antunes, E. and Guedes Soares. C., 2006. Whipping response of vessels with large amplitude motions. In: Proceedings of the 25th International Conference on Offshore Mechanics and Arctic Engineering, (OMAE 2006-92412), Hamburg, Germany.

Gu, M.X., Wu, Y.S. and Xia, J.Z., 1989. Time domain analysis of non-linear hydroelastic response of ships. In: Proceedings of 4th International Symposium on Practical Design of Ships and Other Floating Structures (PRADS). Varna, Bulgaria.

Gu, M.X., Wu, Y.S., and Xia, J.Z., 1988. Time domain analysis of non-linear hydroelastic response of ships. Selected Papers of the Chinese Society of Naval Architecture and Marine Engineering, vol 3. pp. 125–134.

Guedes Soares, C., 1989. Transient response of ship hulls to wave impact. Int. Shipbuild. Progress 36 (406), 137–156.

Guedes Soares, C., 1992. Combination of primary load effects in ship structures. Probab. Eng. Mech. 7, 103–111.

Hirdaris, S.E., Price, W.G., Temarel, P., 2003. Two and three-dimensional hydroelastic modelling of a bulker in regular waves. Mar. Struct. 16 (8), 627–658.

ISSC, 2012. Report of the Technical Committee I.2 on Loads. In: Proc. 18th Int. Ship and Offshore Structures Congress, 1:79-87. Rostock, Germany.

Jensen, J.J., Pedersen, P.T., 1979. Wave-induced bending moments in ships—a quadratic theory. Trans. R. Inst. Nav. Arch. 121, 151–165.

Jensen, J.J., Pedersen, P.T., 1981. Bending moments and shear forces in ships sailing in irregular waves. J. Ship Res. 24 (4), 243–251.

Keane, A.J., Temarel, P., Wu, X.J., Wu, Y., 1991. Hydroelasticity of non-beamlike ships in waves. Trans. R. Soc. Lond. A 334, 187–197.

Mikami, T., Kashiwagi, M., 2008. Time-domain strip method with memory effect functions considering the body nonlinearity of ships in large waves. J. Mar. Sci. Technol. 11 (3), 139–149.

Price, W.G. and Wu, Y.S., 1985. Structural Responses of a SWATH of Multi-Hulled Vessel Traveling in Waves. In: Proceedings of the International Conference on SWATH Ships and Advanced Multi-hulled Vessels. Royal Institution of Naval Architects, London.

Rajendran, S., Fonseca, N., Guedes Soares, C., 2015a. Simplified body nonlinear time domain calculation of vertical ship motions and wave loads in large amplitude waves. Ocean Eng. 107, 157–177.

Rajendran, S., Fonseca, N., Guedes Soares, C., 2016. Body nonlinear time domain calculation of vertical ship responses in extreme seas using a 2nd order Froude–Krylov pressure. Appl. Ocean Res. 54, 39–52.

Rajendran, S., Fonseca, N. and Guedes Soares, C., 2013. Estimation of Short Term Probability Distributions of Wave Induced Loads Acting on a Cruise Vessel in Extreme Seas. In: Proceedings of the 32nd International Conference on Offshore

Mechanics and Arctic Engineering. OMAE 2013-11638.
Rajendran, S., Fonseca, N. and Guedes Soares, C., 2014. Analysis of vertical bending moment on an ultra large containership induced by extreme head seas. In: Proceedings of the 33nd International Conference on Offshore Mechanics and Arctic Engineering. OMAE 2014-24602.
Rajendran, S., Fonseca, N. and Guedes Soares, C., 2015b. Calculation of Vertical Bending Moment Acting on an Ultra Large Containership in Large Amplitude Waves. In: Proceedings of the 34th International Conference on Offshore Mechanics and Arctic Engineering. OMAE 2015-42405.
Ramos, J., Incecik, A., Guedes Soares, C., 2000. Experimental study of slam induced stresses in a containership. Mar. Struct. 13 (1), 25–51.
Santos, F.M., Temarel, P., Guedes Soares, C., 2009a. Modal analysis of a fast patrol boat made of composite material. Ocean Eng. 36 (2), 179–192.
Santos, F.M., Temarel, P.A., Guedes Soares, C., 2009b. On the limitations of two and three-dimensional linear hydroelasticity analyses applied to a fast patrol boat. J. Eng. Marit. Environ. 223 (3), 457–478.
Shi, X., Teixeira, A.P., Zhang, J., Guedes Soares, C., 2016. Reliability analysis of a ship hull structure under combined loads including slamming loading. Ship Offshore Struct. http://dx.doi.org/10.1080/17445302.2014.987438.
Teixeira, A.P., Guedes Soares, C., Chen, N.-Z., Wang, G., 2013. Uncertainty analysis of load combination factors for global longitudinal bending moments of double hull tankers. J. Ship Res. 57 (1), 42–58.
Wang, D.Y., Riggs, H.R., Ertekin, R.C., 1991. Three-dimensional hydroelastic response of a very large floating structure. Int. J. Offshore Polar Eng. 1 (4), 307–316.
Wang, S., Guedes Soares, C., 2013. Slam-induced loads on bow-flared sections with various roll angles. Ocean Eng. 67, 45–57.
Wang, S., Guedes Soares, C., 2014a. Numerical study on the water impact of 3D bodies by an explicit finite element method. Ocean Eng. 78, 73–88.
Wang, S., Guedes Soares, C., 2014b. Comparison of simplified approaches and numerical tools to predict the loads on bottom slamming of marine structures. In: Guedes Soares, C., Lopez Pena, F. (Eds.), Developments in Maritime Transportation and Exploitation of Sea Resources. Taylor & Francis Group, London, UK, pp. 157–170.
Wang, S., Karmakar, D., Guedes Soares, C., 2016. Hydroelastic impact of a horizontal floating plate with forward speed. J. Fluids Struct. 60, 97–113.
Wu, M.K., Moan, T., 1996. Linear and nonlinear hydroelastic analysis of high-speed vessels. J. Ship Res. 40 (2), 149–163.
Wu, Y.S., 1984. Hydroelasticity of Floating Bodies. Brunel University, UK.
Wu, Y.S., Cui, W.C., 2009. Advances in the three-dimensional hydroelasticity of ships. J. Eng. Marit. Environ. 223, 331–348.
Wu, Y.S., Xia, J.Z., Du, S.X., 1991. Two Engineering Approaches to Hydroelastic Analysis of Slender Ships Dynamics of Marine Vehicles and Structures in Waves. Elsevier Science Publishers, Amsterdam, pp. 157–165.
Wu, Y.S., Maeda and H, Kinoshita, T., 1997. The second order hydrodynamic actions on a flexible body. J. Inst. Ind. Sci., Univ. Tokyo 49 (4), 8–19.
Xia, J.Z., Wang, Z.H., Jensen, J.J., 1998. Non-linear wave loads and ship responses by a time-domain strip theory. Mar. Struct. 11 (3), 101–123.
Yamamoto Y, Fujino, M. and Fukasawa T., 1980. Motion and longitudinal strength of a ship in head sea and the effects of non-linearities. Naval Architecture and Ocean Engineering, J Soc Naval Architects of Japan, vol. 18. pp. 91–100.
Zhu, S., Wu, M., Moan, T., 2011. Experimental investigation of hull girder vibrations of a flexible backbone model in bending and torsion. Appl. Ocean Res. 33, 252–274.